Interfacial Stress-Modulated Mechanosensitive Upconversion Luminescence of NaErF$_4$ Based Heteroepitaxial Core–Shell Nanoparticles

Haoqiang Bao, Wang Wang, Xu Li, Xiaomin Liu,* Ling Zhang, Xu Yan, Yinghui Wang, Chenguang Wang, Xiaoteng Jia, Peng Sun, Xianggui Kong, Hong Zhang,* and Geyu Lu*

The resulting interfacial stress in heteroepitaxial nanocomplex usually has negligible influence on its performance, but at high pressures (HP) the effect can be significantly amplified. In order to unravel the underlying mechanism and search for high quality pressure sensors, a simple object is employed, NaErF$_4$@NaLnF$_4$ (Ln = Y, Lu, Gd) and its Tm^{3+}-doped derivatives, to comparatively study the effect of interfacial stress on upconversion (UC) luminescence. Specifically, the doping enhances greatly mechanosensitivity because of the anisotropic local geometry of the dopant ions of which the structural distortion is amplified by HP. The generated compressive strain does extend into the core as witnessed by the effect of tensile strain in the shell on the core and the fact that Lu-shelled nanoparticles are the most sensitive to external force among Tm^{3+}-doped system. This compressive strain in concert with the external HP intensifies the coupling between Er^{3+} and Tm^{3+}, making the attenuation of green UC emission more pronounced. The red to green UC emission ratio of this material, robust both in structural and optical properties, increases linearly with pressure in the range from ambient to 9 GPa. The study opens a new horizon for understanding the effect of interfacial stress on UC luminescence.

1. Introduction

Heterogeneous epitaxial core–shell nanostructures have shown significant advantages in various applications such as luminescence enhancement, bandgap engineering, spectral modulation, multimodal therapeutics, and catalysis.[1–10] During the epitaxial growth of lattice-mismatched materials, the shell lattice needs to adapt to the underlying core lattice structure. When the shell lattice is larger than the core lattice, it will compress, when shell lattice is smaller, it will expand, leading to lattice strain in the epitaxial shell.[11] The strain in the epitaxial shell relaxes beyond a certain thickness, resulting in performance degradation. For instance, the optical performance of semiconductor CdSe nanoparticles (NPs) would be increased by heteroepitaxial growth of CdS or ZnS, but the enhancement is compromised once the shell thickness becomes larger than the critical layer thickness owing to the presence of strain-induced defects.[12,13] Generally, people approved that the lattice mismatch between the core and the shell should be less than 2%, and normally, the design of heteroepitaxial core–shell structures follows this minimum mismatch consideration.[14] However, in the epitaxial shell growth of lanthanide nanostructures, the lanthanide ions have minimal differences in radii and similar chemical properties due to lanthanide contraction, and thus minimal lattice mismatch.[15–19] Different types of heteroepitaxial shell coating all improve the luminescence properties to different degrees, and therefore, the effects of interfacial defects caused by different strains on the optical performance still remain unclear.

H. Bao, X. Li, X. Liu, L. Zhang, X. Yan, C. Wang, X. Jia, P. Sun, G. Lu
State Key Laboratory of Integrated Optoelectronics
Jilin Key Laboratory of Advanced Gas Sensors
College of Electronic Science and Engineering
Jilin University
2699 Qianjin Street, Changchun 130012, China
E-mail: xiaominliu@jlu.edu.cn; lugy@jlu.edu.cn

W. Wang, X. Kong
State Key Laboratory of Luminescence and Applications
Changchun Institute of Optics
Fine Mechanics and Physics
Chinese Academy of Science
Changchun 130033, China

W. Wang, X. Kong
Daheng College
University of the Chinese Academy of Sciences
Beijing 100049, China

Y. Wang
Femtosecond Laser Laboratory
Key Laboratory of Physics and Technology for Advanced Batteries
College of Physics
Jilin University
Changchun 130012, China

H. Zhang
Van't Hoff Institute for Molecular Sciences
University of Amsterdam
Science Park 904, Amsterdam 1098XH, The Netherlands
E-mail: h.zhang@uva.nl

**ADVANCED
SCIENCE NEWS**
www.advancedsciencenews.com

**ADVANCED
OPTICAL
MATERIALS**
www.advopticalmat.de

It is well known that the multicolor luminescence of lanthanide (Ln^{3+}) doped materials upon excitation with near-infrared (NIR) light originates from the intrinsic 4f–4f transitions within the Ln^{3+} ions, which are forbidden in nature by Laporte selection rules. However, by carefully modulating the crystal field environments of the lanthanide ions, the forbidden nature of the UC transitions can be overcome, resulting in long radiative lifetimes (microsecond–millisecond range).[20–22] Since the molecular orbital states involved in lanthanide UC are formed by superimposing the atomic orbitals of the lanthanide ions and those of the host matrix ions, the symmetry of the orbitals can be adjusted by manipulating the geometry of the host lattice.[23] Applying pressure can reduce the distances between the ions/atoms leading to a reduction in the volume of the lattice, a change in the geometry of the crystal, and ultimately a change in optical property.[24–27] The compression of Ln^{3+}-based materials under HP has been reported to lead to the spectral shift of the absorptions and emissions, change of intensities, band broadening, as well as change of luminescence lifetimes,[28–35] owing to the enhanced energy migration rates, cross-relaxation (CR) and multiphonon relaxation processes. Inspired by this, it can be reasonably inferred that it is feasible to use HP as a mean to amplify the influence of different interface strains on luminescence.

In this work, we adopted two types of heteroepitaxial core–shell structure $NaErF_4@NaLnF_4$ and its related derivatives $NaErF_4$:0.5% $Tm@NaLnF_4$ (Ln = Y, Lu, Gd). $NaErF_4@NaLnF_4$ is a pure system characteristic of i) different interfacial strains (tensile strain in Lu shell, compressive strain in Y and Gd shell) and ii) fast energy transfer rates and abundant CR processes attributed to the strong correlation of the energy level of Er^{3+} ions. Besides these two characteristics, $NaErF_4$:0.5% $Tm@NaLnF_4$ is also subject to additional lattice doping perturbation. 0.5% Tm^{3+} ions provide an alternative energetic pathway which siphons would-be photons from Er^{3+} ions green states into the red state.[36,37] Thus, applied forces change not only the external crystal field of the ions but also the coupling of energy between Er^{3+} and Tm^{3+} ions. We have comparatively studied the laws of different interfacial strains on the luminescence of these two systems under atmospheric and HP conditions. Our research highlights how the different interfacial strains in concert with the external pressure-induced lattice shrinkage modulate the UC luminescence properties and the mechanosensitivity to pressure.

2. Results and Discussion

2.1. Synthesis

First, $NaLnF_4$ (Ln: Y, Lu, Gd) precursor was synthesized by an existing procedure,[38,39] then the $NaErF_4$ and $NaErF_4$:0.5% Tm bare cores were synthesized by the previously reported method with some modifications.[40] and finally the $NaErF_4@NaLnF_4$ and $NaErF_4$:0.5% $Tm@NaLnF_4$ (Ln: Y, Lu, Gd) upconversion nanoparticles (UCNPs) were synthesized by the Ostwald ripening method.[38] Details on synthesis materials and methods are in the Supporting Information.

2.2. Characterization and Analysis of UCNPs

Figure 1 illustrates the formation of core–shell structure of $NaErF_4@NaLnF_4$ (Ln = Y, Lu, Gd) and $NaErF_4$:0.5% $Tm@NaLnF_4$ (Ln = Y, Lu, Gd), respectively. First, $NaErF_4$ core NPs and $NaErF_4$:0.5% Tm core NPs were synthesized under the same condition following chloride thermal decomposition approach,[40] which ensures that different shells can be better grown on the same core and conducive to comparison among core–shell samples. The $NaErF_4$ and $NaErF_4$:0.5% Tm core NPs are uniform in size, with an average size of 20.7 ± 1.3 and 20.5 ± 1.4 nm, respectively. Transmission electron microscope (TEM) graphs in Figure 1a show the morphology of $NaErF_4$ core coated with different inert shell $NaLnF_4$ (Ln = Y, Lu, Gd), denoted as Er@Y, Er@Lu, and Er@Gd, which have average diameters of 40.9 ± 2.0 nm (Y), 40.1 ± 2.1 nm (Lu), and 43.2 ± 2.0 nm (Gd), respectively. Figure 1b shows the morphology of $NaErF_4$:0.5% Tm core coated with different inert shell $NaLnF_4$ (Ln = Y, Lu, Gd), denoted as Er:Tm@Y, Er:Tm@Lu, and Er:Tm@Gd, with average particle sizes of 40.2 ± 1.9 nm (Y), 39.4 ± 2.1 nm (Lu), and 40.5 ± 1.8 nm (Gd) respectively. Figure 1c,d shows the elementary distribution mapping of these two types of core–shell NPs, from which it can be seen that the core element (Er) is distributed inside the NPs, while the shell elements (Y, Lu, and Gd) are distributed in the outer layer of the NPs, demonstrating the successful manufacture of the core–shell structure. These two types of core–shell materials (Er@Ln and Er:Tm@Ln, Ln = Y, Lu, Gd) have nearly identical dimensions, 10 nm shell thickness, good monodispersity and hexagonal disk shape. Based on this success, the structure, luminescence properties at atmospheric and variable pressures, sensitivity to mechanical stress can be studied and compared.

To examine the effect of heteroepitaxial growth on the structure, we characterize the synthesized samples by X-ray diffraction (XRD). **Figure 2**a,d shows the diffraction peaks of Er@Ln and Er:Tm@Ln (Ln = Y, Lu, Gd), respectively, which match the standard hexagonal structure of $NaErF_4$ (JCPDs. No:27-0689). However, a detailed observation at individual peak reveals lattice changes caused by different interfacial strains and heteroepitaxial growth. From the (201) crystal plane enlargements of Er@Ln and Er:Tm@Ln (Ln = Y, Lu, Gd) core–shell NPs (Figure 2b,e), it is clearly seen that the peaks of the Y-shelled and Gd-shelled NPs shift toward the smaller 2θ angle, while the Lu-shelled NPs shift toward the large 2θ angle. Smaller 2θ angles are related to larger d-spacings, vice versa. The ionic radius of Lu^{3+} ion in **Table 1** is 2.4% smaller than that of Er^{3+} ion, so the Lu-shell needs to be tensile to adapt to the Er-based core. Similarly, the ionic radius of Y^{3+} ion and Gd^{3+} ion are 1.3% and 4.3% larger than that of Er^{3+} ion, respectively, so the Y-shelled and Gd-shelled need to be compressive to adapt to the Er-based core. The lattice constants of two types of core–shell NPs from the data of (101) and (201) diffraction peaks are calculated from the reported equations (Equation (S1), Supporting Information),[41] with the results given in **Table 2**. In the system with $NaErF_4$ core, the lattice constants a of core, Y-shelled, Lu-shelled, and Gd-shelled NPs are 5.959, 5.999, 5.954, and 6.061 Å, respectively, corresponding to the relevant mismatch to the core in lattice constant a of +0.67%, −0.08%, and +1.71%. The lattice constants c of core, Y-shelled, Lu-shelled, and
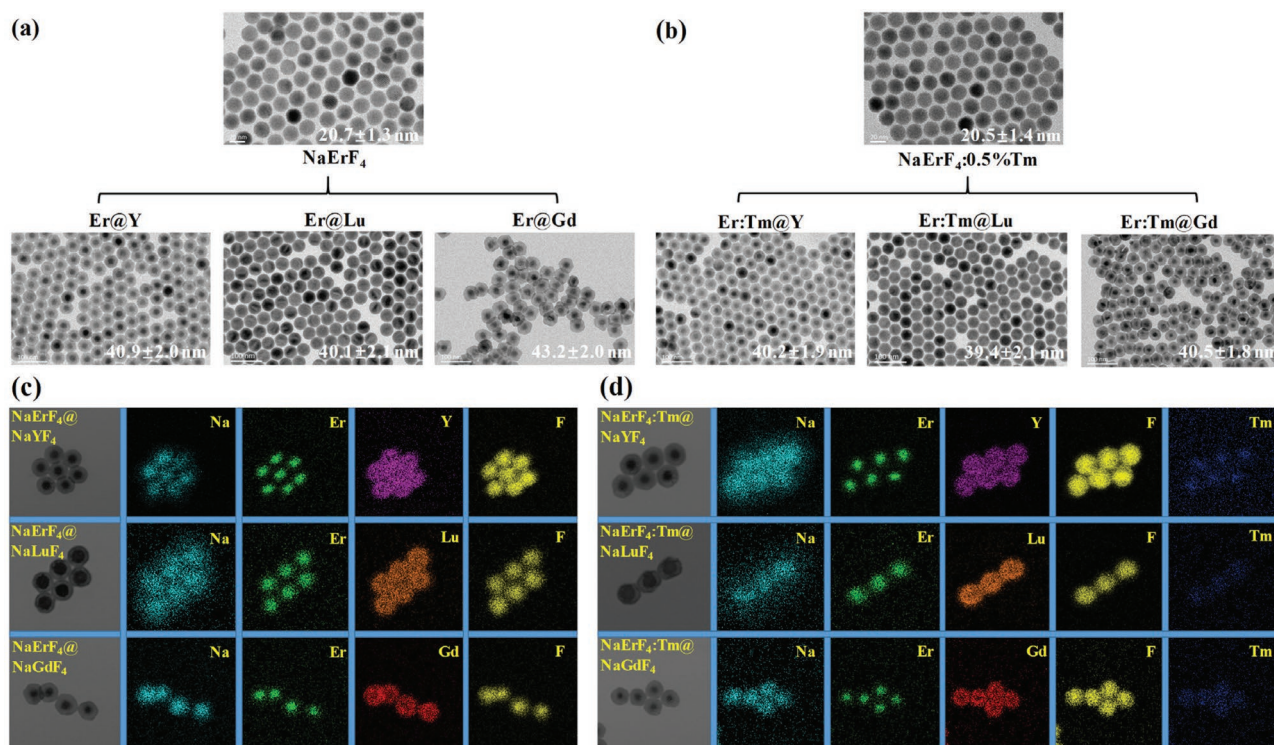
Figure 1. Micrographs and elemental distribution mapping of core–shell NPs. a,b) The top two pictures are the TEM of the $NaErF_4$ and $NaErF_4$:0.5% Tm bare core NPs, the scale bar is 20 nm. The bottom six pictures are the TEM of the $NaErF_4@NaLnF_4$ and $NaErF_4$:0.5% Tm@$NaLnF_4$ (Ln = Y, Lu, Gd) core–shell NPs, the scale bar is 100 nm, the average sizes or diameters of core and core–shell NPs are given in the pictures. c,d) The elemental distribution mapping of the $NaErF_4@NaLnF_4$ and $NaErF_4$:0.5% Tm@$NaLnF_4$ (Ln = Y, Lu, Gd) core–shell NPs.

Gd-shelled NPs are 3.487, 3.510, 3.479, and 3.549 Å, respectively., corresponding to the relevant mismatch to the core in lattice constant c of +0.66%, −0.23%, and +1.78%. Obviously, Lu-shelled NPs have the smallest mismatch. The same trend is also observed in Er:Tm@Ln (Ln = Y, Lu, Gd) system. That is, among these heterogeneous shell materials, the Lu shell has the smallest lattice mismatch. The result shows that the tensile strain causes highly isotropic NPs compared with the compressive strain.[11] Therefore, the $NaLuF_4$ shell with tensile stress maintains the closest approximation to the homogeneous epitaxial growth, leading to minimal interface defects.

This conclusion is further confirmed by the steady-state UC emission of these two types of core–shell materials. Figure 2c,f indicates the UC spectra of Er@Ln and Er:Tm@Ln (Ln = Y, Lu, Gd) at atmospheric pressure with a constant excitation power density of 10 W cm^{-2} at 980 nm excitation. It is found that $NaLuF_4$ as an inert shell harvests the brightest UC emission for both Er@Ln and Er:Tm@Ln (Ln = Y, Lu, Gd) systems. The same is true for 808 and 1530 nm excitations (Figure S1, Supporting Information).

2.3. Emission Detection and Analysis of Er@Ln and Er:Tm@Ln UCNPs under HP

To explore the mechano-optical properties of these core–shell NPs, the powder core–shell NPs were added into a 200 µm diameter sample chamber of the diamond anvil cell (DAC) with

a needle under a microscope, silicon oil and ruby (**Figure 3**a) were also added to the sample chamber. Silicon oil was used to maintain the quasihydrostatic environment, while ruby was used to provide pressure calibration. Lasers with wavelengths of 808, 980, and 1530 nm were used to excite the NPs in the DAC and monitored the UC emission. A wrench was used to pressurize the DAC manually.

UC luminescence was recorded for Er@Ln and Er:Tm@Ln (Ln = Y, Lu, Gd) (Figure 3b) under different pressures ranging from 0 to 9 GPa at 980 nm excitation. Figures S2 and S3 (Supporting Information) are pressure-dependent UC luminescence spectra under 808 and 1530 nm excitation. The integrated luminescence intensities of Er@Ln and Er:Tm@Ln (Ln = Y, Lu, Gd) core–shell materials continuously decrease with the pressure increases, regardless of the type of shell coating, indicating that HP increases the possibility of multiphoton relaxation (higher phonon energy and larger electron–phonon coupling), cross-relaxation (shorter distance between ions), and nonradiative energy transfer of NPs.[23,30,33] In addition, the possible strains and defects formed in the crystal by the pressurization process also contribute to the luminescence quenching.

Now we turn to the spectral shape change. The reaction of pressure on the red-to-green ratio of Er@Ln and Er:Tm@Ln (Ln = Y, Lu, Gd) core–shell materials was studied. The red-to-green ratios of all core–shell NPs exhibit different degrees of increase with increasing pressure (**Figure 4**). For clarity, the UC spectra are normalized at 541 nm (green) and 652 nm (red) at variable pressure, respectively, in Figures S4–S6

ADVANCED
SCIENCE NEWS
www.advancedsciencenews.com

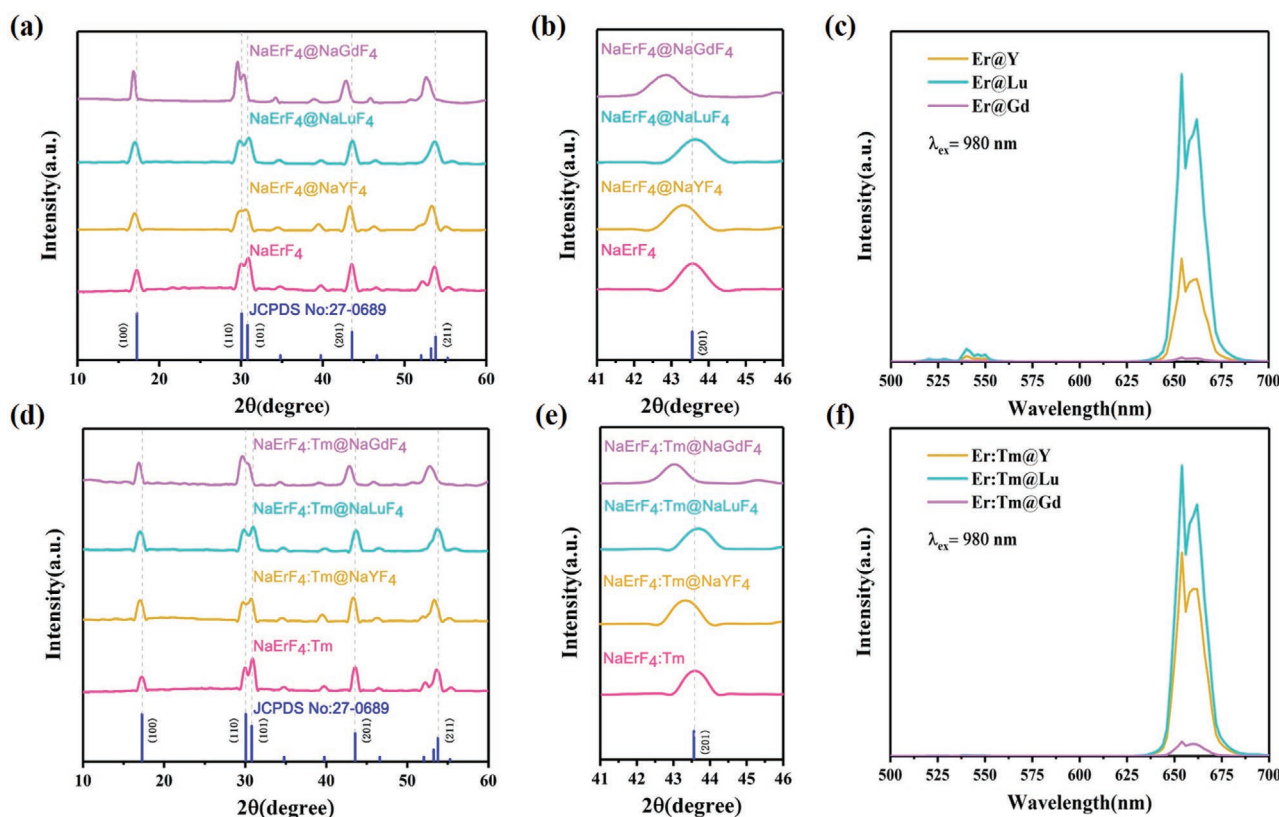ADVANCED
OPTICAL
MATERIALS
www.advopticalmat.de

Figure 2. Structure characterization and UC luminescence monitoring of NPs under atmospheric pressure. a) The picture shows the relevant powder XRD diffraction patterns of the $NaErF_4$ bare core (pink), Er@Y (orange), Er@Lu (cyan), and Er@Gd (purple), the standard hexagonal structure of $NaErF_4$ NPs (JCPDS No: 27-0689) is taken as a comparison. b) A zoom-in of the (201) diffraction peak shows a shifting in the 2θ angle position between $NaErF_4$ and $NaErF_4$@NaLnF$_4$ (Ln = Y, Lu, Gd) NPs. c) The picture shows the UC emission spectra of $NaErF_4$@NaLnF$_4$ (Ln = Y, Lu, Gd) NPs by 980 nm excitation (10 W cm^{-2}). d–f) The pictures show the same issues as picture a–c) except that the $NaErF_4$ core is replaced by the $NaErF_4$:0.5% Tm core.

(Supporting Information). It can be said although the intensities of green and red UC emission decrease with the increase of pressure (Figure 3b), the green UC emission diminishes more rapidly than the red UC emission, resulting in an increase in the red-to-green ratio. The green UC emission of Er^{3+} ions is more sensitive to external force, a phenomenon also reported in other literature.[29,30]

We quantify the mechanosensitivity of nanoparticles by analyzing the linear response of the red-to-green ratio ($I_{(r)}/I_{(g)}$) to pressure. Specifically, the change in the red-to-green ratio per unit pressure ($\Delta I_{(r)}/I_{(g)}$) is defined by the slope calculated from the linear fit, and the mechanosensitivity is responded by the slope value. Taking 980 nm excitation as an example, it can be seen from Figure 4 that the slopes of Y-shelled, Lu-shelled, and Gd-shelled NPs in the Er@Ln (Ln = Y, Lu, Gd) system are 0.35, 0.37, and 0.46 GPa^{-1}, respectively. The slopes of Y-shelled, Lu-shelled, and Gd-shelled NPs in the Er:Tm@Ln (Ln = Y, Lu, Gd) system are 1.37, 3.76, and 1.82 GPa^{-1}, respectively. It is

obvious that the slopes of the Er:Tm@Ln (Ln = Y, Lu, Gd) system are generally larger than those of Er@Ln (Ln = Y, Lu, Gd), indicating that the Er:Tm@Ln (Ln = Y, Lu, Gd) system is more sensitive to pressure. In other words, the pressure has a greater effect on the doped system compared to the undoped system.

In the case of Er:Tm@Ln (Ln = Y, Lu, Gd) doped system, Er^{3+} ions act as dual functions of energy harvesting and emission. Upon direct 980 nm excitation as indicated in Figure S7a (Supporting Information) (the energy transfer diagram under 808 and 1530 nm excitations are given in Figures S7b and S8c, Supporting Information), photons populate the $^4I_{11/2}$ energy level of Er^{3+} ions (Step 1). Subsequently, due to the characteristics of the energy structure of Tm^{3+}, it facilitates the energy transfer from the $^4I_{11/2}$ and $^4I_{13/2}$ energy levels of Er^{3+} ions down to the $^3H_5$ and $^3F_4$ energy levels of Tm^{3+} ions, respectively (Step 2). Thus, a large amount of excitation energy is transferred from Er^{3+} ions to the Tm^{3+} ions, which effectively reduces the loss of energy caused by rapid migration to the particle surface or internal lattice defects. The energy stored in Tm^{3+} will then promote the population of the red-emitting $^4F_{9/2}$ energy level of Er^{3+} ions via energy transfer UC (Step 3), achieving robust monochromic red UC emission (Step 4).[36,37,42] Therefore, the doping of Tm^{3+} ions can increase the $I_{(r)}/I_{(g)}$, and it is confirmed from Figure 4 that the $I_{(r)}/I_{(g)}$ of Tm^{3+} ions doped system is larger than that of undoped system. On the other hand, the pressure shortens

Table 1. The ionic radius and ionic mismatch of lanthanide ions from Gd^{3+} ion to Lu^{3+} ion.

Ionic	Gd^{3+}	Y^{3+}	Er^{3+}	Tm^{3+}	Lu^{3+}
Ionic radius [Å]	1.193	1.159	1.144	1.134	1.117
Ionic mismatch	−4.3%	−1.3%	0	+0.9%	+2.4%

Table 2. Summary of structural information for core–shell NPs.

Sample	Lattice Constant a [Å]	Lattice Constant a mismatch[a]	Lattice Constant c [Å]	Lattice Constant c mismatch[a]
NaErF$_4$ core	5.959	–	3.487	–
NaYF$_4$ shelled	5.999	+0.67%	3.510	+0.66%
NaLuF$_4$ shelled	5.954	−0.08%	3.479	−0.23%
NaGdF$_4$ shelled	6.061	+1.71%	3.549	+1.78%
NaErF$_4$:0.5%Tm core	5.942	–	3.487	–
NaYF$_4$ shelled	5.993	+0.86%	3.511	+0.69%
NaLuF$_4$ shelled	5.926	−0.27%	3.478	−0.26%
NaGdF$_4$ shelled	6.036	+1.58%	3.535	+1.38%

[a]The negative and positive signs indicate compressive and tensile strain at the shell, respectively.
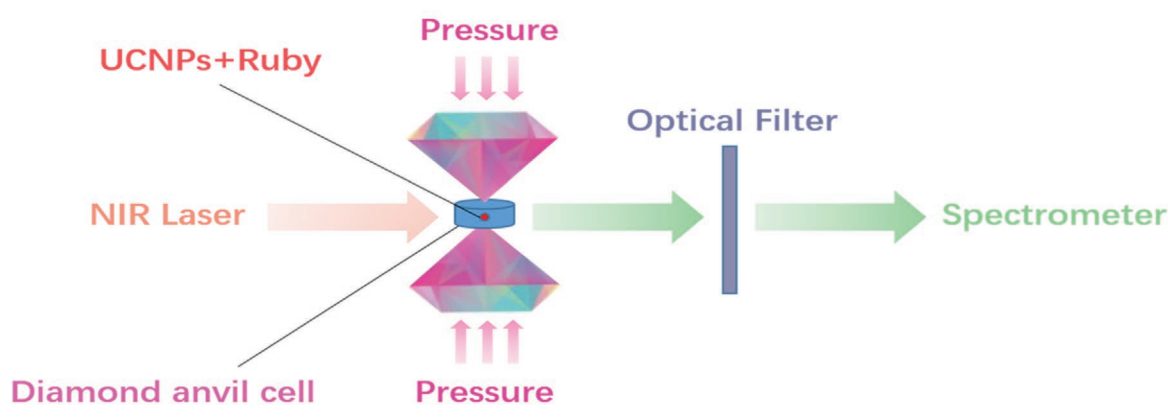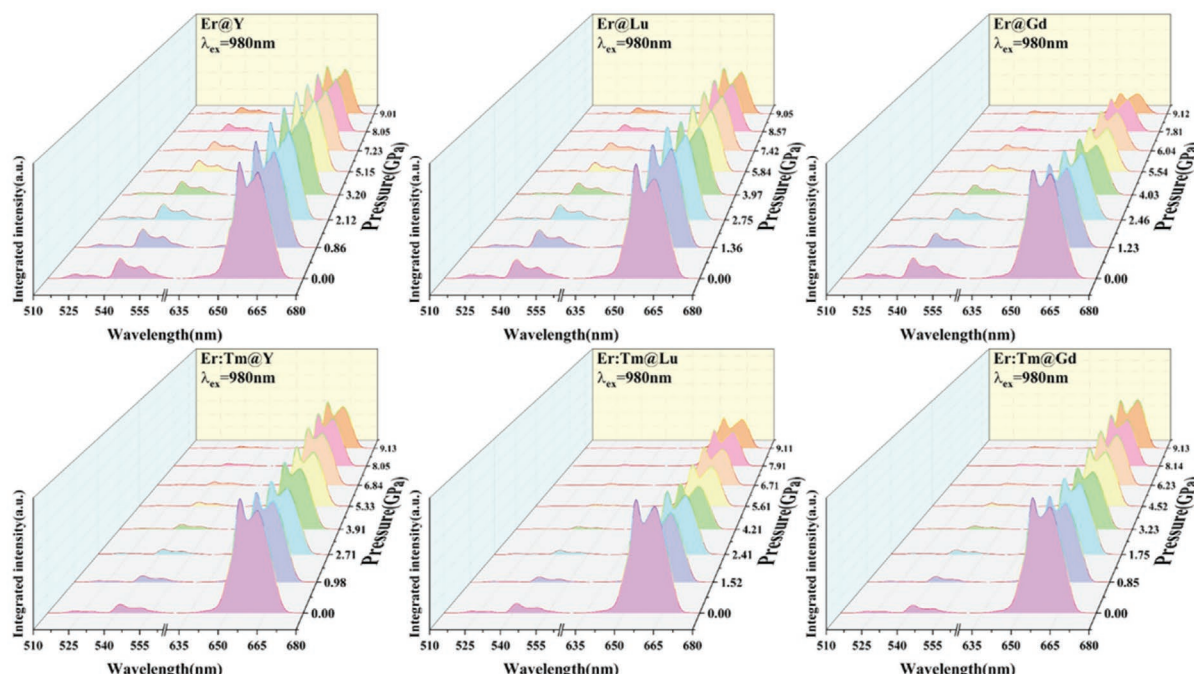

Figure 3. Emission detection of NPs under HP. a) UCNPs and ruby are inserted into the sample volume of the DAC and compressed. (the ruby was used to provide pressure calibration) NPs in DAC are excited by 808, 980, and 1530 nm lasers, respectively, and the emission light is collected by the spectrometer after passing through the optical filter. b) The UC emission spectra of NaErF$_4$@NaLnF$_4$ core–shell NPs (the top three pictures) and NaErF$_4$:0.5% Tm@NaLnF$_4$ (Ln = Y, Lu, Gd) core–shell NPs (the bottom three pictures) under the pressure from 0 to 9 GPa by 980 nm excitation.
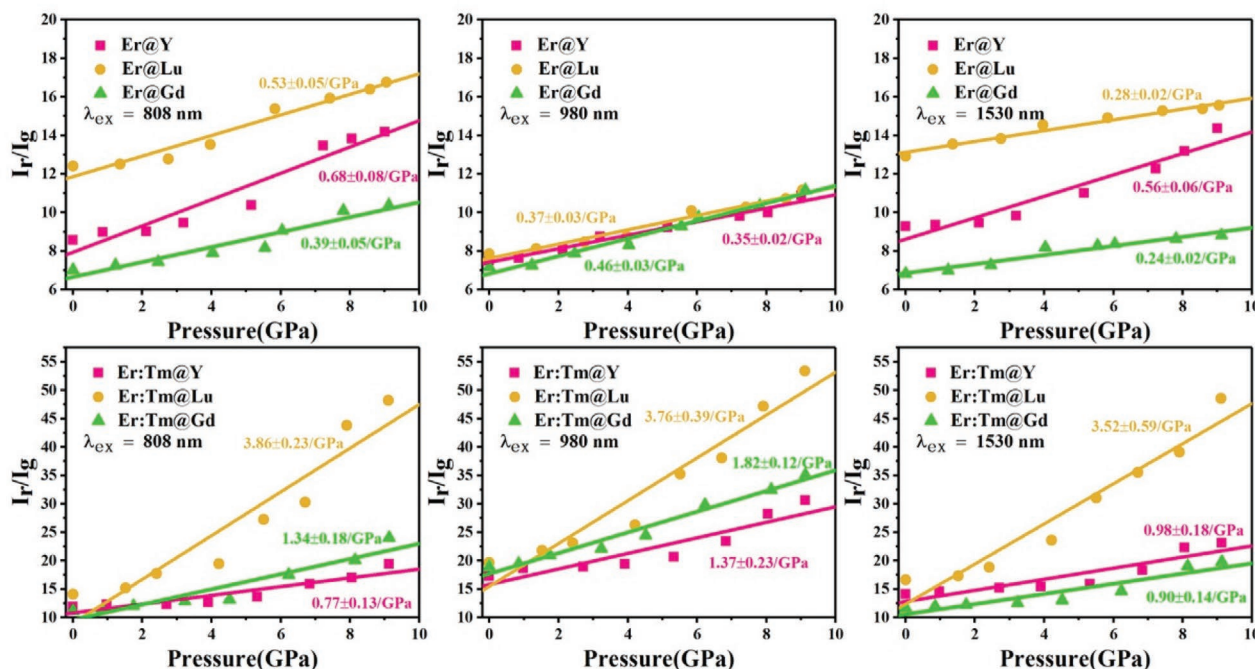
Figure 4. Mechanosensitivity response of core–shell NPs. The ordinate in the picture represents the ratio of the red light integral area to the green light integral area in the emission spectrum of NPs, which is represented by $I_{(r)}/I_{(g)}$. The pictures reflect the change of $I_{(r)}/I_{(g)}$ of $NaErF_4@NaLnF_4$ and $NaErF_4$:0.5% $Tm@NaLnF_4$ (Ln = Y (pink), Lu (yellow), Gd (green)) NPs with pressure. Each group of points in the pictures are fitted linearly and the number represents the slope of the line, slope values reflect the mechanosensitivity of NPs.

the bonds only in undoped crystals without altering the coordination-environment symmetry, whereas, in doped crystals, the local geometry around Er^{3+} ions are inhomogeneous and thus this structural distortion can be amplified under HP, which increases the crossover of the electron cloud density of Er^{3+} ions and Tm^{3+} ions, resulting in enhanced coupling between the Er^{3+} ions and Tm^{3+} ions,[31] making the $\Delta I_{(r)}/I_{(g)}$ larger in the doped system than in the undoped system.

For Er@Ln (Ln = Y, Lu, Gd) system, the slopes do not change much regardless of whether the compressive strain (Y and Gd-shelled NPs) or the tensile strain (Lu-shelled NPs) in the shell, indicating that different interfacial strains do not affect the undoped system much in compressed materials. However, for the Er:Tm@Ln (Ln = Y, Lu, Gd) system, the slopes of the Y-shelled and Gd-shelled NPs with the compressive strain in the shell are close to each other, with slopes of 1.37 and 1.82 GPa^{-1}, respectively if the 980 nm excitation is taken as an example. While the slope of Lu-shelled NPs with the tensile strain in the shell increases sharply with a slope value of 3.76 GPa^{-1} (Figure 4), demonstrating that the Lu-shelled NPs have the most responsiveness to external stress. As shown in Figure S8 (Supporting Information), this enhanced response suggests that tensile strain in the shell affects the mechanosensitivity of the core by way of generating compressive strain that extends into the core. This compressive force of the core further increases the coupling between Er^{3+} ion and Tm^{3+} ion which better plays the role of Tm^{3+} ion in trapping, storing, and transferring energy, making the attenuation of green light more pronounced, increasing the $\Delta I_{(r)}/I_{(g)}$. This inference can be demonstrated by the pressure-dependent green

UC emission reduction rate of Er:Tm@Ln (Ln = Y, Lu, Gd) NPs. As indicated in **Table 3**, the reduction rates of green UC emission of Lu-shelled NPs, $NaErF_4$:0.5% $Tm@NaLuF_4$, are significantly greater than those of Y-shelled and Gd-shelled NPs. We also measured the HP UC emission and quantified the corresponding mechanosensitivity of $NaErF_4$:0.5%$Tm@NaLuF_4$ NPs with various thicknesses (6, 12, and 18 nm), as indicated in Figure S9 (Supporting Information), there is no significant difference in the mechanosensitivity of nanoparticles with different shell thicknesses.

2.4. Detection and Analysis of $NaErF_4$:0.5% $Tm@NaLuF_4$ NPs under HP Cycles

We analyze the mechanosensitivity of $NaErF_4$:0.5% $Tm@NaLuF_4$ NPs specifically by comparing the UC luminescence spectra at atmospheric pressure (pink) and the highest pressure (yellow) as indicated in **Figure 5**a–c. Each spectrum is normalized according to the green UC emission to highlight the variation of the red UC emission relative to the green UC

Table 3. Summary of the green emission reduction rates of the Tm^{3+} ion doped system.

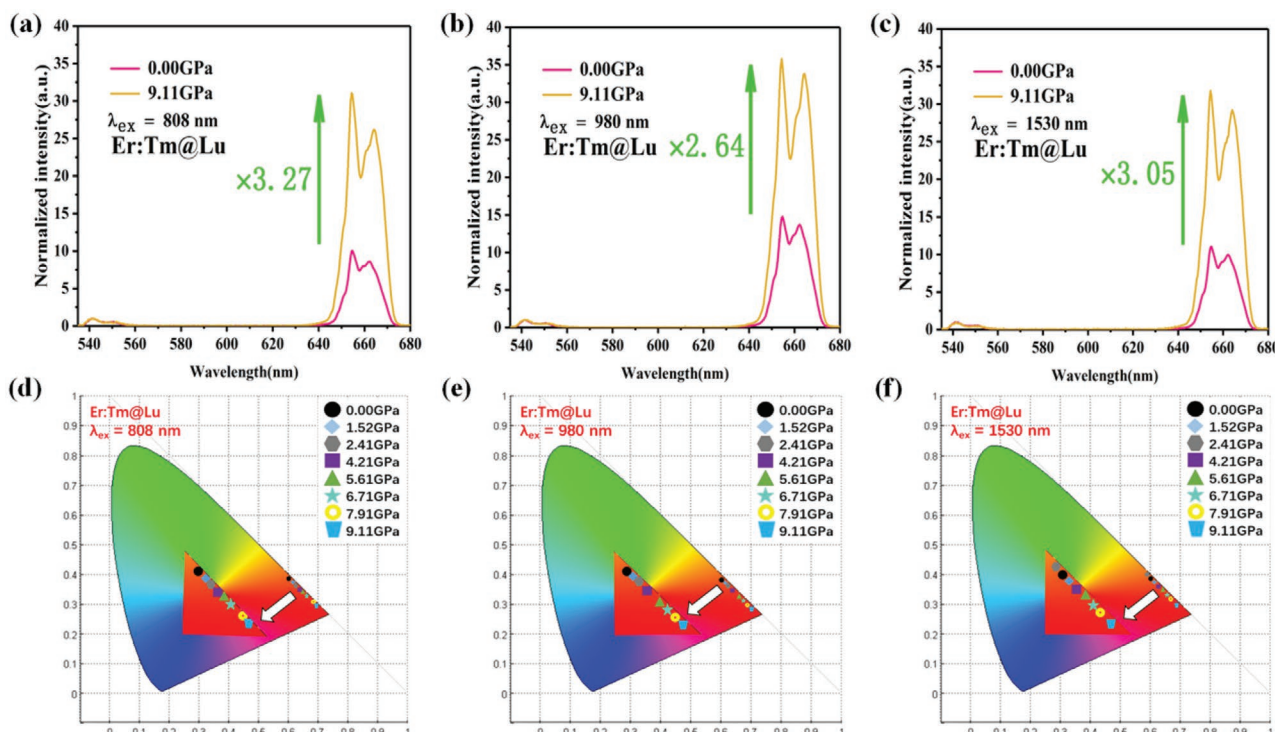| Sample [nm]	Er:Tm@Y (green)	Er:Tm@Lu (green)	Er:Tm@Gd (green)
λ_{ex} = 808	-0.79 ± 0.14	-1.05 ± 0.17	-0.77 ± 0.14
λ_{ex} = 980	-0.75 ± 0.14	-1.07 ± 0.14	-0.79 ± 0.14
λ_{ex} = 1530	-0.70 ± 0.13	-1.10 ± 0.17	-0.67 ± 0.13

Figure 5. Color response of Er:Tm@Lu NPs to pressure. a–c) Each emission spectrum is normalized to its own green emission peak, the pictures reflect the increasing multiple of the red light integral intensity under 0 GPa (pink) and 9.11 GPa (yellow), the enhancements of red light are ×3.27, ×2.64, and ×3.05 under a) 808 nm, b) 980 nm, and c) 1530 nm excitation, respectively. d–f) The chromaticity coordinate diagrams of the NPs were plotted by CIE 1931, and the emitting color changes of Er:Tm@Lu NPs with increasing pressure were analyzed under d) 808 nm, e) 980 nm, and f) 1530 nm excitation, respectively.

emission. It can be found that the integrated intensity of red UC emission at the highest pressure is significantly enhanced compared to the atmospheric pressure, with the enhancements of ×3.27, ×2.64, and ×3.05 under 808, 980, and 1530 nm excitation, respectively. We plot the chromaticity coordinate diagram (Figure 5d–f) based on the HP UC emission spectra of $NaErF_4$:0.5% Tm@$NaLuF_4$ NPs. The luminescent color of NPs gradually changed from orange-red to dark red with pressure increasing. It is also found that the luminescence color of NPs changes with pressure in a large span under different excitations, demonstrating that $NaErF_4$:0.5% Tm@$NaLuF_4$ NPs can be used for mechanical sensing where the doped Tm^{3+} ion energetic coupling with the emitter Er^{3+} ion is tunable by external pressure, leading to perceivable and measurable color changes.

Through further tracking, it can be seen that $\Delta\ I_{(r)}/I_{(g)}$ of the two complete compression and release periods (from 0 to 9 GPa) changes with the ambient values. The following equation is used to perform the linear fitting for each period

$$\log\left[I_{(r)}/I_{(g)}\right] = K_* P + B \tag{1}$$

K is the slope of the fitting curve, which reflects the mechanosensitivity of $NaErF_4$:0.5% Tm@$NaLuF_4$ NPs. The higher the absolute value of K, the greater the color response of the NPs to stress. P is the external pressure, which ranges from 0 to 9 GPa. B is a constant, reflecting the $I_{(r)}/I_{(g)}$ of NPs under atmospheric pressure. As shown in **Figure 6**a–c, the logarithm

of the red-to-green ratio of $NaErF_4$:0.5% Tm@$NaLuF_4$ NPs has a linear relationship with pressure. As can be seen in Table S1 (Supporting Information), the mechanosensitive values K of NPs has no significant decline in the cycles of compression and release, indicating the structural and optical robustness of these NPs for multiple pressure measurements. Figure 6d; and Figure S10a (Supporting Information) describe the luminescence integral intensity of red and green UC emission of NPs with pressure in the two cycles of compression and release, where the UC emission intensity can be restored to the initial value after release. Figure 6e; and Figure S10b (Supporting Information) are the spectral shift of each UC emission peak during the compression and release cycles. The peak positions of the red and green UC emission hardly change during the cycle which implies that the crystal structures of NPs do not change under HP. We also tested the XRD, TEM, and photoluminescence results after releasing pressure. As can be seen in Figure S11 (Supporting Information), the crystal structure, morphology, and UC emission property of the NPs remain the same as their initial state. In summary, $NaErF_4$:0.5% Tm@$NaLuF_4$ NPs have good mechanosensitive and optical stability and thus is an ideal material for HP calibration.

3. Conclusion

In conclusion, we systematically study how the different interfacial strains in concert with the external pressure-induced lattice
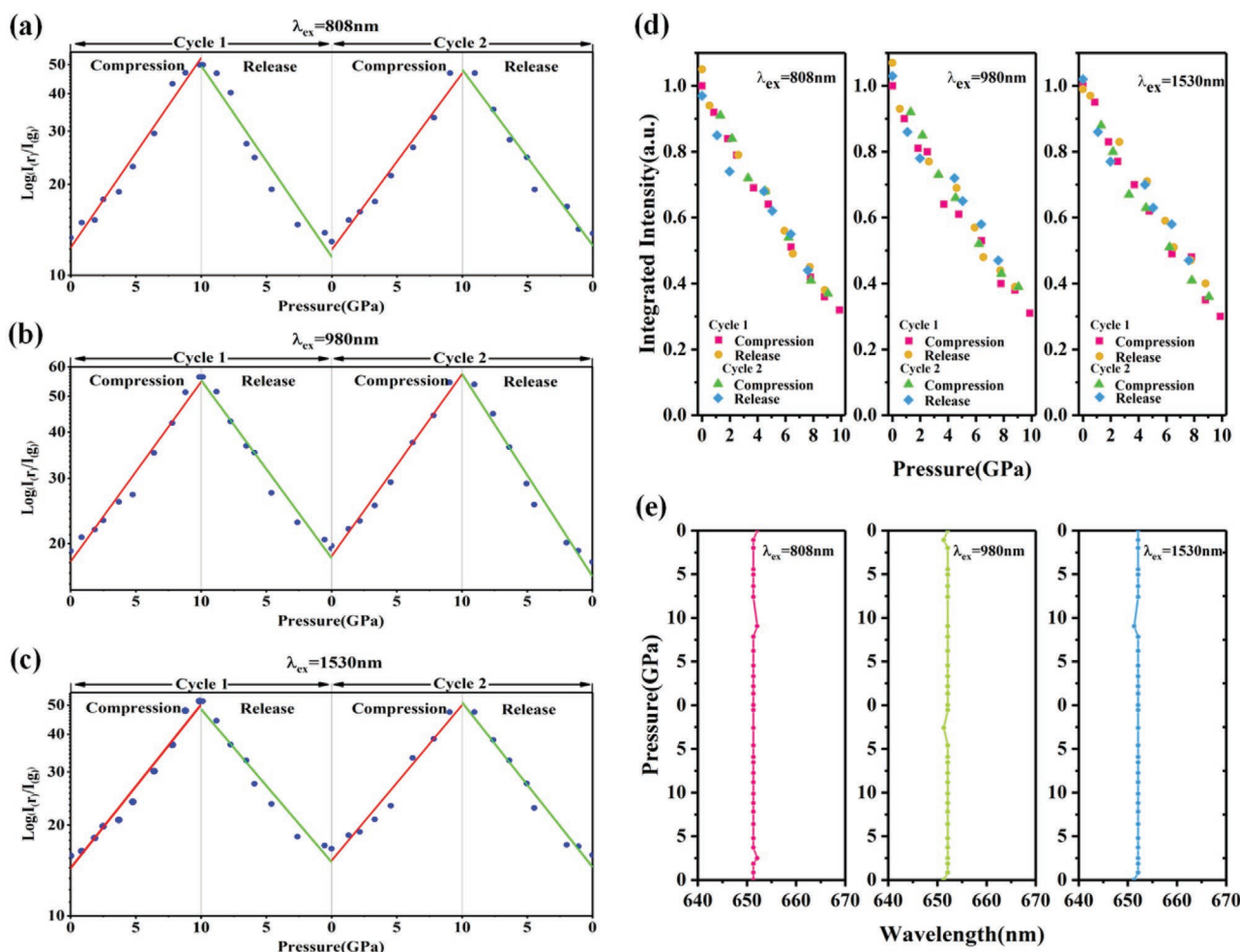
Figure 6. Detection and analysis of Er:Tm@Lu NPs under HP cycle. Mechanosensitive response of Er:Tm@Lu NPs monitored from the intensity ratio of the red and green UC emission. Excitation is at a) 808 nm, b) 980 nm, and c) 1530 nm. Straight lines are the fitting results of the experimental data during pressure (red) and release (green) with Equation (1). d) Integrated UC emission normalized to the initial value of red emission at different excitation wavelengths. The pink square, yellow circle, green triangle, and blue diamond represent the cycle 1 pressurization, cycle 1 release, cycle 2 pressurization, and cycle 2 release processes, respectively. e) The peak position of the red emission at different excitation wavelengths during the two cycles.

shrinkage modulate the UC luminescence properties and the mechanosensitive to pressure. Heteroepitaxial core–shell structure Er@Ln and its relevant derivatives Er:Tm@Ln (Ln = Y, Lu, Gd) are adopted as simple objects. At atmospheric pressure, the $NaLuF_4$ shell coating with tensile stress tends to produce isotropic nanostructures in contrast to the shell with compressive stress, and thus Lu-shelled nanoparticles harvest the strongest UC luminescence. The externally applied HP causes the UC emission of both systems to diminish. However, the Tm^{3+}-doped system is generally more mechanosensitive than the undoped system under HP, regardless of the interfacial stress. Because HP only shortens the distance in undoped systems, but the local geometry around Er^{3+} ions is inhomogeneous in the doped system, HP amplified this structural distortion. In addition, among the Tm^{3+}-doped system, Lu-shelled NPs ($NaErF_4$:0.5% $Tm@NaLuF_4$) with tensile stress are the most sensitive to external force, suggesting that tensile strain in the shell influences the mechanical sensitivity of the core by way of generating compressive strain that extends into the core. This compressive strain in concert with the external HP further intensifies the coupling between Er^{3+} and Tm^{3+}, making the attenuation of green UC emission more pronounced. The red to green UC emission ratio increases linearly with pressure in the range from ambient to 9 GPa, yielding an observed color change from orange-red to dark red. Moreover, the changing pattern remains consistent in the cycles of compression and release, suggesting that the emission intensity can be restored to the initial value after pressure release with stable structural and optical properties. These properties allow the material to be used for high pressure calibration. Our study also sheds a light on understanding the effect of interfacial stress on UC luminescence.

Supporting Information

Supporting Information is available from the Wiley Online Library or from the author.

[1] J. Zhang, Y. Tang, K. Lee, O. Min, *Science* **2010**, *327*, 1634.
[2] S. E. Habas, H. Lee, V. Radmilovic, G. A. Somorjai, P. Yang, *Nat. Mater.* **2007**, *6*, 692.
[3] L. Carbone, P. D. Cozzoli, *Nano Today* **2010**, *5*, 449.
[4] B. Chen, Y. Wang, Y. Guo, P. Shi, F. Wang, *ACS Appl. Mater. Interfaces* **2021**, *13*, 2327.
[5] B. Zhou, L. Yan, J. Huang, X. Liu, L. Tao, Q. Zhang, *Nat. Photonics* **2020**, *14*, 760.
[6] B. Zhou, B. Tang, C. Zhang, C. Qin, Z. Gu, Y. Ma, T. Zhai, J. Yao, *Nat. Commun.* **2020**, *11*, 1174.
[7] S. Wen, Y. Liu, F. Wang, G. Lin, J. Zhou, B. Shi, Y. D. Suh, D. Jin, *Nat. Commun.* **2020**, *11*, 6047.
[8] H. Li, X. Wang, X. Li, S. Zeng, G. Chen, *Chem. Mater.* **2020**, *32*, 3365.
[9] J. Zuo, D. Sun, L. Tu, Y. Wu, Y. Cao, B. Xue, Y. Zhang, Y. Chang, X. Liu, X. Kong, W. J. Buma, E. J. Meijer, H. Zhang, *Angew. Chem., Int. Ed.* **2018**, *57*, 3054.
[10] J. Zuo, L. Tu, Q. Li, Y. Feng, I. Que, Y. Zhang, X. Liu, B. Xue, L. J. Cruz, Y. Chang, H. Zhang, X. Kong, *ACS Nano* **2018**, *12*, 3217.
[11] N. J. J. Johnson, F. C. J. M. F. Van Veggel, *ACS Nano* **2014**, *8*, 10517.
[12] J. McBride, J. Treadway, L. C. Feldman, S. J. Pennycook, S. J. Rosenthal, *Nano Lett.* **2006**, *6*, 1496.
[13] X. B. Chen, Y. B. Lou, A. C. Samia, C. Burda, *Nano Lett.* **2003**, *3*, 799.
[14] Z. L. Wang, *J. Phys. Chem. B* **2000**, *104*, 1153.
[15] N. J. J. Johnson, F. C. J. M. Van Veggel, *Nano Res.* **2013**, *6*, 547.
[16] Y. Zhang, X. Zhu, Y. Zhang, *ACS Nano* **2021**, *15*, 3709.
[17] Z. Yuan, L. Zhang, S. Li, W. Zhang, M. Lu, Y. Pan, X. Xie, L. Huang, W. Huang, *J. Am. Chem. Soc.* **2018**, *140*, 15507.
[18] C. Liu, B. Liu, J. Zhao, Z. Di, D. Chen, Z. Gu, L. Li, Y. Zhao, *Angew. Chem., Int. Ed.* **2020**, *59*, 2634.
[19] J. Zhao, X. Chen, B. Chen, X. Luo, T. Sun, W. Zhang, C. Wang, J. Lin, D. Su, X. Qiao, F. Wang, *Adv. Funct. Mater.* **2019**, *29*, 1903295.
[20] P. A. Tanner, *Chem. Soc. Rev.* **2013**, *42*, 5090.
[21] W. Zheng, P. Huang, D. Tu, E. Ma, H. Zhu, X. Chen, *Chem. Soc. Rev.* **2015**, *44*, 1379.
[22] T. C. Brunold, H. U. Güdel, *Inorganic Structure and Spectroscopy*, Wiley-Interscience, New York **1999**.
[23] M. D. Wisser, M. Chea, Y. Lin, D. M. Wu, W. L. Mao, A. Salleo, J. A. Dionne, *Nano Lett.* **2015**, *15*, 1891.
[24] C. Gong, Q. Li, R. Liu, Y. Hou, J. Wang, X. Dong, B. Liu, X. Yang, Z. Yao, X. Tan, D. Li, J. Liu, Z. Chen, B. Zou, T. Cui, B. Liu, *Phys. Chem. Chem. Phys.* **2013**, *15*, 19925.
[25] W. Li, X. Ren, Y. Huang, Z. Yu, Z. Mi, N. Tamura, X. Li, F. Peng, L. Wang, *Solid State Commun.* **2016**, *242*, 30.
[26] J. S. Wang, C. L. Ma, D. Zhou, Y. S. Xu, M. Z. Zhang, W. Gao, H. Y. Zhu, Q. L. Cui, *J. Solid State Chem.* **2012**, *186*, 231.
[27] L. Wang, L. Yang, Y. Ding, Y. Ren, S. Xiao, B. Liu, S. V. Sinogeikin, Y. Meng, D. J. Gosztola, G. Shen, R. J. Hemley, W. L. Mao, H.-K. Mao, *Phys. Rev. Lett.* **2010**, *105*, 095701.
[28] M. A. Antoniak, S. J. Zelewski, R. Oliva, A. Zak, R. Kudrawiec, M. Nyk, *ACS Appl. Nano Mater.* **2020**, *3*, 4209.
[29] A. Lay, O. H. Sheppard, C. Siefe, C. A. McLellan, R. D. Mehlenbacher, S. Fischer, M. B. Goodman, J. A. Dionne, *ACS Cent. Sci.* **2019**, *5*, 1211.
[30] A. Lay, C. Siefe, S. Fischer, R. D. Mehlenbacher, F. Ke, W. L. Mao, A. P. Aliyisatos, M. B. Goodman, *Nano Lett.* **2018**, *18*, 4454.
[31] A. Lay, D. S. Wang, M. D. Wisser, R. D. Mehlenbacher, Y. Lin, M. B. Goodman, W. L. Mao, J. A. Dionne, *Nano Lett.* **2017**, *17*, 4172.
[32] M. Runowski, J. Marciniak, T. Grzyb, D. Przybylska, A. Shyichuk, B. Barszcz, A. Katrusiak, S. Lis, *Nanoscale* **2017**, *9*, 16030.
[33] M. Runowski, A. Shyichuk, A. Tyminski, T. Grzyb, V. Lavin, S. Lis, *ACS Appl. Mater. Interfaces* **2018**, *10*, 17269.
[34] P. Wozny, M. Runowski, S. Lis, *J. Lumin.* **2019**, *209*, 321.
[35] K. Zhang, C. Gao, Z. Jiang, Y. Wei, Y. Pan, C. Wei, H. Li, K. Wang, B. Zou, L. Huang, *Adv. Opt. Mater.* **2020**, *8*, 1901031.
[36] E. M. Chan, G. Han, J. D. Goldberg, D. J. Gargas, A. D. Ostrowski, P. J. Schuck, B. E. Cohen, D. J. Milliron, *Nano Lett.* **2012**, *12*, 3839.
[37] Q. Chen, X. Xie, B. Huang, L. Liang, S. Han, Z. Yi, Y. Wang, Y. Li, D. Fan, L. Huang, X. Liu, *Angew. Chem., Int. Ed.* **2017**, *56*, 7605.
[38] N. J. J. Johnson, A. Korinek, C. Dong, F. C. J. M. Van Veggel, *J. Am. Chem. Soc.* **2012**, *134*, 11068.
[39] H. X. Mai, Y. W. Zhang, L. D. Sun, C. H. Yan, *J. Phys. Chem. C* **2007**, *111*, 13730.
[40] Z. Li, Y. Zhang, *Nanotechnology* **2008**, *19*, 345606.
[41] W. Wang, Z. Feng, B. Li, Y. Chang, X. Li, X. Yan, R. Chen, X. Yu, H. Zhao, G. Lu, X. Kong, J. Qian, X. Liu, *J. Mater. Chem. B* **2021**, *9*, 2899.
[42] J. Zuo, Q. Li, B. Xue, C. Li, Y. Chang, Y. Zhang, X. Liu, L. Tu, H. Zhang, X. Kong, *Nanoscale* **2017**, *9*, 7941.